This article has been accepted for publication in a future issue of this journal, but has not been fully edited. Content may change prior to final publication. Citation information: DOI 10.1109/JRFID.2020.3011900, IEEE Journal of Radio Frequency Identification

Passive UHF RFID Voice Prosthesis Mounted Sensor for Microbial Growth Detection

V Makarovaite*, A Hillier †, S J Holder †, C W Gourlay †, J C Batchelor †

**University of Kent, UK and vm255@kent.ac.uk, †University of Kent, UK*

***Abstract*—Capacitive loading due to human tissue can lead to low efficiency for implantable Passive Radio Frequency Identification (RFID) antennas. The presented passive UHF antenna sensor provides read distances above 0.5 meters (within a body phantom) by utilizing a convoluted half-wave dipole design. It is able to detect simulated early to mature *Candida albicans* biofilm growth when mounted upon a voice prosthesis (up to a 30 µm biofilm thickness). Depending on the propagation frequency of interest, as early 4-hour growth (5 to 10 µm biofilm thickness) equivalent could be detected and before any device failure could occur due to the colonization. This was accomplished by utilising thin layers of polyurethane to decouple the saliva from the presented UHF sensor (biofilm growth is known to increase layer hydrophobicity). This presented sensor has better functionality within the US UHF frequency band as it detects changes above 5 µm. If there is a need for implantation within additional tissues with variable dielectric properties, a shunt capacitance of 2.6 pF could allow the system functionality within the permittivity range of 21 to 58. Allowing for immediate medical intervention before medical prosthesis failure.**

Keywords— UHF, Implantable, Design, Sensor, Microbial detection

I. INTRODUCTION

There is a global market projected increase of US$3.9 billion in the 'next generation implants' by 2023 worth an estimated US$141 billion [1, 2]. Increased global utilization of medical implants should be coupled with an increase in expected implant complications of which the majority (20 to 25%) is composed of microorganism colonization of device surfaces (or adjacent host tissues) [3]. However, the overall infection rate for medical implants (when grouped together) is only near 2%; the infection rate exponentially increases (near 50%) for temporary devices such as catheters [4]. Microorganism colonisation on medical devices often leads to device failure necessitating implant removal (and often replacement), increasing costs and straining often underfunded healthcare organizations [3].

This is commonly seen in laryngectomy patients requiring a voice prosthesis device for speaking assistance [4]. The fungal species *Candida albicans* is often the main cause of voice prosthesis failure as it is a common oral opportunist pathogen able to form a multi-layer biofilm [4-6]. Currently, there is no method for early *C. albicans* growth detection prior to device failure or patient infection symptoms occurring [3-6]. Overall, necessitating the need for real-time prosthetic device microbial growth detection (within a host) to limit the cost of implant failure and often replacement upon global healthcare systems. Passive ultra-high frequency (UHF) radio frequency identification (RFID) technology is a possible option for this type of wireless real-time detection providing relatively unobtrusive sensor capabilities; hopefully, limiting the unnecessary cost linked with prosthetic device failure and removal by allowing for early failure detection due to microbial growth. There has been some work on varying RFID systems able to sense microbial growth, but none have looked at biofilm formation for common oral pathogens such as *C. albicans* [7-11].

Passive RFID technology functions by receiving an incoming signal from the reader antenna often as a continuous wave which undergoes a backscatter modulation received by a reader antenna. Many versions of passive RFID sensors exist (magnetic resonance, thickness shear mode, inductor-capacitor-resistor transducers (LRCs) and etc.) [7]. 'Self-sensing' RFID sensors are recommended to reduce the cost and obstructiveness of additional lumped components (capacitors, resistors and inductors) often employed in matching networks [12]. The 'self-sensing' methodology relies on modifications in the geometrical or physical appearance of an RFID design to tune the signal modulation seen by an antenna reader [12]. This approach has limitations in sensing capabilities as it is limited by the prosthetic dimensions, antenna read distance and market available integrated circuits (ICs) to achieve any noticeable changes due to microbial growth. However, this approach is recommended as a cost-effective limited use strategy for devices able to detect microbial growth before a host exhibits symptoms of infection requiring hospitalization and/ or treatment.

Copper etched 'self-sensing' LRC circuit design can lessen the costs associated with UHF RFID fabrication while reducing human tissue capacitive loading effect by etching inductive or capacitive components within the design geometry [7, 12]. The presented design is an adjusted version of [13] first presented in the RFID-TA 2019 conference [14]. The original design was chosen as it provided high read ranges (above 4 meters) and a known functionality within high dielectric solutions equivalent to human tissues (2 to 80 permittivity). The presented etched resonating loop dipole antenna was matched to a Higgs-3 Gen 2 RFID IC (31- j216 Ω at 865 MHz) [15]. The final design was a half-wave dipole sensor with a 22 mm diameter, 14 mm height and a dipole length near 50 mm (Fig. 1B). Current sensor was etched in copper and covered in polymer but any future utilization for human use would require silver or any other human tissue safe metal with similar conductivity to copper. We present the antenna function within a gelatine and salt human neck phantom and any simulated adjustments needed for microbial growth sensing within the neck or other device implantation sites.

II. METHODS

UHF RFID read range determines the performance of a proposed design; the antenna reader in passive systems

This article has been accepted for publication in a future issue of this journal, but has not been fully edited. Content may change prior to final publication. Citation information: DOI 10.1109/JRFID.2020.3011900, IEEE Journal of Radio Frequency Identification

provides the necessary minimum 'wake-up' for activation of an IC. The common formula utilized for RFID maximum read range is calculated by:

$$r_{max} = \frac{\lambda}{4\pi}\sqrt{\frac{QG_{rd}G_{tg}P_{rd}}{P_{tg}}} \quad (1)$$

where the abbreviations correlate with tag gain (G_{tg}), reader gain (G_{rd}), reader frequency (λ), impedance mismatch factor (Q), tag received power (P_{tg}) and reader power (P_{rd}) [12]. Within antenna sensor design, only adjustments to tag gain (G_{tg}) and the quality factor (Q) will affect read range as the other properties are determined by the antenna reader and transponder IC manufacturers as well as UHF band country regulations [12]. Unlike UHF holds preference to HF (high-frequency) designs due to the ability to increase matched system data rate transfers, higher gain as well as increased read ranges [16]. Utilising read range can allow sensitive sensor development as presented below in this extended version of the RFID-TA conference paper [14].

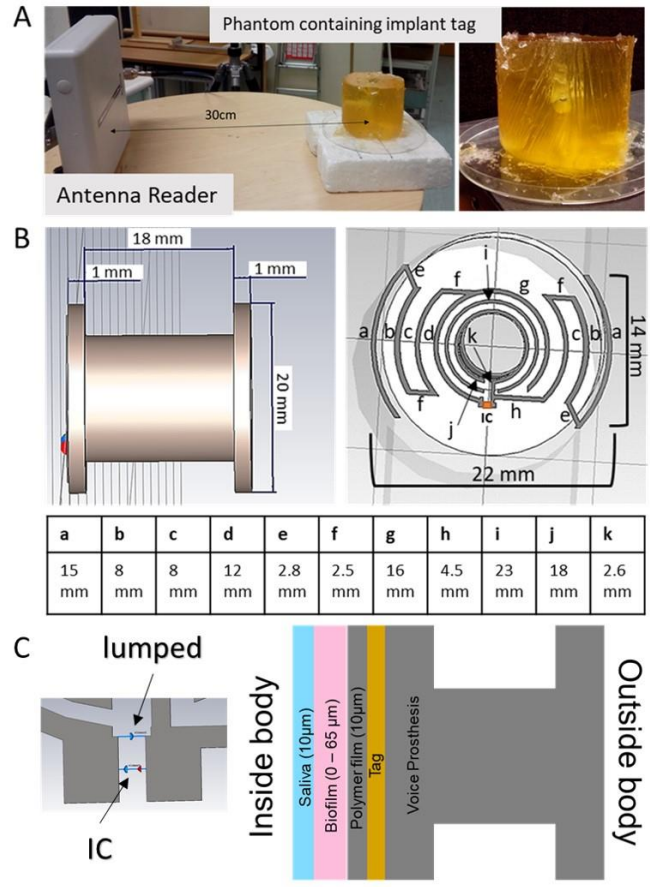

a	b	c	d	e	f	g	h	i	j	k
15 mm	8 mm	8 mm	12 mm	2.8 mm	2.5 mm	16 mm	4.5 mm	23 mm	18 mm	2.6 mm

Figure 1 UHF RFID voice prosthesis sensor design implanted within a neck phantom. A) The reader antenna calibration with a 30 cm separation between the sensor and antenna within the neck phantom (salt and gelatine); and B) The tag and sensor dimension upon the voice prosthesis model utilised for data collection. C) Exhibits the lumped element placement and IC location as well as the sketched view of the represented layers involved in the device simulation. *The same neck phantom dimensions were utilized within the CST simulations and TagformancePro measurements.*

A. Experiment Design:

To account for biofilm development on the voice prosthesis (including a layer of polymer and saliva), a 2.2 pF capacitor shunt was included in the simulation to tune the frequency resonance within the desired EU UHF frequency band (near 865 MHz). The presented sensor faces towards the midline of the simulated trachea (wind-pipe) (Fig. 1) as the damaging *C. albicans* growth is prevalent at this location leading to device failure [7]. Most commonly, the movable phalange (which allows air movement through the device and speech) fails due to microbial overgrowth [7]. The method for determine the capacitance was same as describe in [13] except for the additional lumped capacitance attached (in parallel) to the simulated IC component. It should be noted that saliva has a high dielectric constant and the detuning effect induced by the neck phantom and saliva must be understood before the shunt capacitance can be calculated as seen in [13].

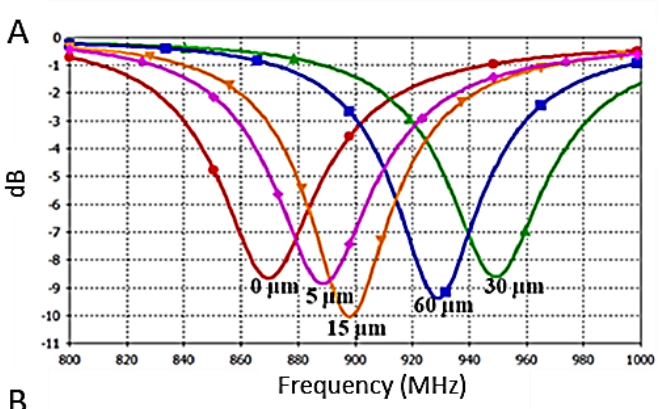

B

"Biofilm Thickness		No Growth	5 µm	15 µm	30 µm	60 µm
Resonant Frequency (MHz)		868	889	898	949	928
Capacitance at Resonance (x 10^{-11})		1.7	1.5	2.1	1.5	1.7
Impedance at Resonance	Real	56	53	50	55	52
	Imaginary	-10	-12	-8	-11	-9.9

Figure 2 S11 simulated *C. albicans* biofilm growth on the A) antenna sensor and b) simulated matching parameter changes due to increase in biofilm thickness. Till a mature biofilm layer is reached (30 µm thickness), there is a noticeable resonant frequency increase. Once the mature layer thickness doubles in height a top the sensor, there is a reversal in resonant frequency likely due to the saliva decoupling.

Overall, the simulated design (Fig. 2) consisted of a single polymer layer (CST library lossy silicone thickness ranging from 10 µm to 75 µm) topped with a 10µm saliva layer; both layers had the same diameter to the voice prosthesis modelled of 20 mm. However, the 10 µm layer was considered as no growth layer as *C. albicans* is unable to grow on metal *in vivo*. Therefore, the actual growth ranged from 0 µm to 65 µm thickness as the 0 µm thickness (no growth) includes the 10 µm polymer coating needed for *C. albicans* growth to occur. This is the same experimental methodology as presented in [14]. Also, most studies show that early *C. albicans* biofilm growth corresponds to a thickness near 30 µm and below 100 µm before biofilm shedding occurs [3-6]. Therefore, simulated values at or below 100 µm thickness are utilized. Polymer was used to simulate biofilm growth as it has been shown that biofilm matrices become highly hydrophobic overtime [3-6]. This hydrophobicity is linked with a loss in conductivity in the surrounding fluid equivalent to an increase in polymer layer thickness calculated based on the effect on a known system (xCELLigence) [17]. However, mature bacterial biofilms are much thinner than fungal *C. albicans* biofilms as such the thickness of the simulated layer was increased as stated previously [3-6, 17].

Also, dielectric tissue measurements (SPEAG Dak Dielectric Probe [18]) of volunteer necks exhibited a negligible variability in both permittivity and conductivity (±2.31 permittivity and 0.64±0.058 conductivity) (Table I). According to [19], neck musculature does not share a proportional relationship with increasing body size and

This article has been accepted for publication in a future issue of this journal, but has not been fully edited. Content may change prior to final publication. Citation information: DOI 10.1109/JRFID.2020.3011900, IEEE Journal of Radio Frequency Identification

weight; small variability exists within the volunteer population even with increasing fat to muscle ratios. Ultimately, allowing for the use of a single salt and gelatine neck phantom to encompass a wide variety of BMI values ranging from 20.8 to 44.9 (Table I). Suggesting that UHF sensor development, localized within the human neck, only requires a single phantom for modelling the high dielectric neck tissue.

TABLE I. SPEAG Probe Dielectric Properties of Volunteer Necks (865 MHz)

BMI	***Permittivity (293.75 K)***	***Conductivity (S/m)***	***tan(δ)***
20.8	40.30 ± 0.19	0.63± 0.007	0.33±0.003
44.9	40.29±0.68	0.60±0.20 0	0.31±0.005
26.1	42.70±0.77	0.72±0.017	0.35±0.003
20.5	36.75±1.14	0.58±0.030	0.33±0.007
Average	**40.1±2.31**	**0.64±0.058**	**0.33±0.015**

Table II information was collected (using the same Dak measurement probe) from volunteer forearms (a decidedly variable location between individuals). The forearm is an easy site for data collection, which can help simulate a broader range of dielectric properties between real human tissue; placement of sensor within any other location of the body would require an adjustment. To show the effect of this on sensor properties, the simulation was re-run using volunteer (non-neck body) dielectric data to help visualize the effect of altering phantom dielectric properties. Simulated dielectric variability would determine the effect of sensor implantation within human tissues in varying locations on the body (Table II). Also, it should help determine additional adjustments needed to remain within a regulated ETSI frequency band.

TABLE II. SPEAG Probe Dielectric Properties of Volunteer Forearms and Human Saliva (865 MHz)

	Permittivity (294.25 K)	***Conductivity (S/m)***	***BMI***
Volunteer 1	22.5 ± 0.02	0.26± 0.020	20.8
Volunteer 2	31.0 ± 0.55	0.42± 0.189	26.7
Volunteer 3	42.2± 0.23	0.67 ± 0.051	24.3
Saliva	39.8 ± 0.98	0.3 ± 0.012	x
Gelatine phantom	58 ± 0.04	1.0 ± 0.002	x

B. Sensor Measurements:

An empirical study was conducted on the presented prototype to evaluate the accuracy of the simulated model as well as to determine the actual functionality of the sensor. A neck (gelatine and salt) phantom was developed, able to mimic human tissue based on the Dak dielectric measurements [20]. This produced a 10 cm diameter and 20 cm height phantom with human muscle equivalent dielectric properties (Table II). The CST simulations had the exact same design for a neck phantom and use of gelatine dielectric properties. This was done to increase the correlation of tag efficiency and directivity in comparison to the measured data. However, to mimic the effect of changing dielectric properties and insertion within a volunteer, a separate CST simulation also included a head phantom and chest block (underneath and above the neck phantom) made of the same material and double the dimensions (Fig. 5 only). This was merely done to determine the detuning effect of additional tissues (head and torso) as well as excessive changes in tissue dielectric properties. All other CST simulations and measurements only utilized the gelatine and salt neck phantom.

The antenna sensor was read with the TagformancePro Voyantic RFID antenna measurement system and repeated in triplicate [21]. The frequency was swept at 5 MHz frequency steps and 0.1 dBm power steps between 800 to 1000 MHz frequency range. Also, the power was kept below 30 dBm to keep within the determined human safe power levels. For calibration, the equipment was set at 30 cm distance separating the antenna reader and sensor tag (Fig. 1 A). An increase in a polyurethane layer on top of the sensor region was included to mimic *C. albicans* biofilm growth. The measured layers ranged from 0 to 50 µm for normal 48-hour growth and an excessive growth layer of 100 µm were included. Before measurements were taken, a thin layer of saliva on top of the polyurethane (around 10 µm thickness) was added with a pipette to simulate a human throat environment. For each reading and replicate data, the saliva layer was adjusted to remain near a 10 µm thickness. All readings were repeated in triplicate and read quickly as to maintain saliva layer integrity.

This was also done in order to determine the necessary thickness of a polymer layer able to reduce the capacitive loading of high dielectric saliva layer upon the sensor region of the presented UHF design. For simulation simplification purposes, this polymer layer was kept at 10 µm (0 growth) as stated previously however, no such separate layer was included in the TagformancePro actual measured values. It is expected that the measured values will correspond with the simulations suggesting a 10 µm as the minimum polymer layer to increase sensor sensitivity to less than 40 µm (mature *C. albicans* biofilm). The 10 µm layer in the measured results corresponds to 0 µm growth of the simulated results and, therefore, the 10 to 40 µm of the measured data is equivalent to 0 to 30 µm growth of the simulated data.

III. RESULTS

The transponder IC showed a 90% power transfer for the convoluted dipole presented with a -20.57 dB total efficiency in the EU frequency band (867 MHz specifically). However, a -20 dB total efficiency is common due to power dissipation when UHF antennas are placed within (or upon) high dielectric human tissue. Regardless of the reduced total efficiency, the presented antenna sensor was able to produce above a 50 cm read range for both the 865 MHz (65 cm) and 920 MHz (80 cm) frequency bands (Fig. 3 A). Additionally, there was limited variability in read distance between the triplicate repeats.

When looking at the CST simulations, an increase in *C. albicans* biofilm thickness resulted in a noticeable frequency shift. This was likely due to the saliva layer decoupling from the antenna parasitic loop region which resulted in the saliva layer being further decoupled with the increasing thickness of the polymer layer. This decoupling would then result in increased hydrophobicity of the polymer layer as the saliva is further decoupled, mimicking the expected biofilm growth. Based on simulations, biofilm growth of 5 µm thickness should be detectable upon the voice prosthesis while within the neck phantom. However, a thickness of 10 µm or less was equated to 'no growth' as a layer of polymer is necessary to allow any true biofilm attachment and formation. These simulations also exhibited the expected change within the sensor capacitance resulting in resonant frequency increase (Fig. 2B); IC matching was highly affected by the decoupling of the saliva resulting in a capacitance shift. Ultimately, the

This article has been accepted for publication in a future issue of this journal, but has not been fully edited. Content may change prior to final publication. Citation information: DOI 10.1109/JRFID.2020.3011900, IEEE Journal of Radio Frequency Identification

decoupling of the saliva from the antenna functions similarly to what is common within other wearable antenna designs when viewed at a single frequency and the antenna itself is moved further from the human body (high conductivity and permittivity) [22]. As this is a first attempt to understand the effect of saliva and microbial growth on UHF RFID sensor design, further study is necessary.

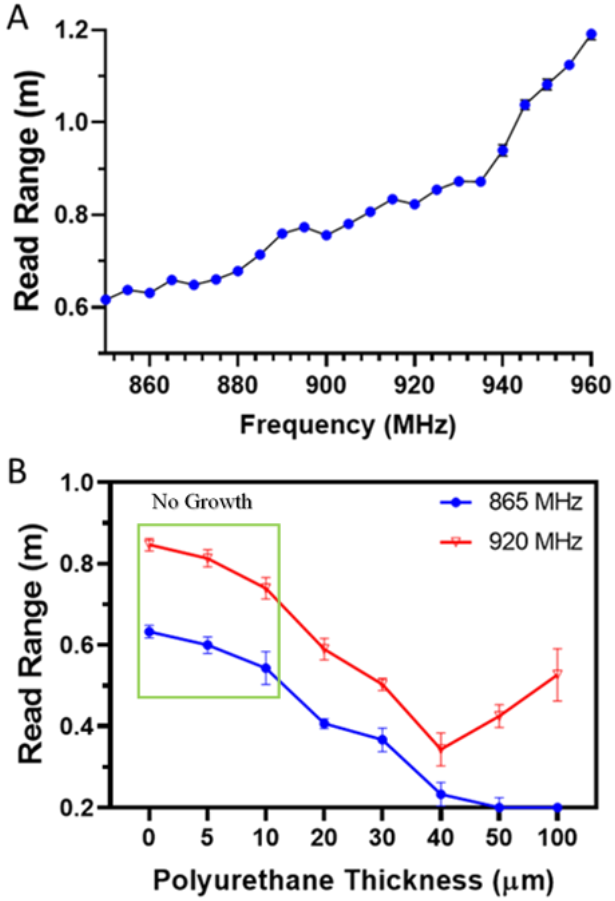

Figure 3 Measurement of sensor function mounted on voice prosthesis within a salt and gelatine neck phantom. A) Antenna measurement over both the EU and USA UHF frequency bands without any biofilm growth adjustments (0 µm polyurethane thickness). B) Sensor function at both the EU (865 MHz) and USA (920 MHz) UHF frequency bands with biofilm layer adjustment to mimic *C. albicans* growth overtime on the voice prosthesis.

When the UHF sensor was tested utilising a salt and gelatine neck phantom, an additional capacitance shunt adjustment was found to not be necessary as the design was able to produce a read range above 0.5 meters (Fig. 3A) with the addition of 10 µm layer of saliva. Therefore, it was decided that a less obtrusive design would be preferable to the addition of lumped elements; particularly, as only one design would be necessary for the high dielectric of human neck tissues as seen in Table I. However, unlike the CST simulations, a significant difference between 0 and 5 µm layer thickness was not present nor between 5 and 10 µm for 865 MHz values. There however was a significant difference above 10 µm till 40 µm suggesting that the polymer layer before growth should be set at a minimum of 10 µm (as shown in Fig. 2 and 3).

Similarly, with 920 MHz there was also no significant difference between 0 and 5 µm; however, there was a significant variance above 5 µm till 40 µm (Fig. 3B). It should be noted that as seen within the simulations (Fig. 2), there was a reversal in read range above 40 µm within the 920 MHz frequency band; however, not in 865 MHz (Fig. 3B). This corresponds with the reversal in the frequency shift above 40 µm; As the polymer layer increases the frequency shifts upwards before there is a reversal and the frequency shifts to account for the change in capacitance on the sensor.

This also suggests that to increase the sensitivity of this sensor for measuring biofilm growth, a minimum of 10 µm polymer layer must be included to decouple the saliva from the sensor. This should be enough to increase the sensor sensitivity (at both EU and USA UHF bands) as the sensor was able to easily sense additional thickness above this first polymer layer. If this is done, then the sensor will have the same sensing capability as the simulation of 0 to 30 µm above the incorporated 10 µm polymer layer. However, unlike the simulations, this shown no need for the additional 2.2 pF shunt as it worked above 0.5 m without it. This is understandable as CST software is not ultimately made for body implantable UHF devices and can (from empirical studies) underestimate the read distance and radiation efficiency for such simulations. Therefore, everything must be evaluated with real measurements and not rely on simulations alone.

Antenna matching is affected by both conductivity and permittivity of the surrounding environment [23]; as conductivity drops (seen in a biofilm growth from no growth (0 µm) to mature (30 µm)), the S11 matching is reduced while a change in permittivity results in a shift in resonant frequency rather than just efficiency. Both a shift in frequency and S11 matching can be seen in the simulations suggesting that biofilm growth is a combination of both these properties within the simulated biofilm environment (Fig. 2). However, permittivity is expected to play a greater role (at least till a mature thickness is reached) as there is a greater change seen in resonant frequency than S11 matching alone (Fig. 2A). The estimated directivity exhibited a unidirectional pattern with an 86° main lobe direction and a 2.31 dBi directivity magnitude (Fig. 4). This was expected for an implantable UHF passive sensor as all simulated biofilm thickness remained near -20% total efficiency range.

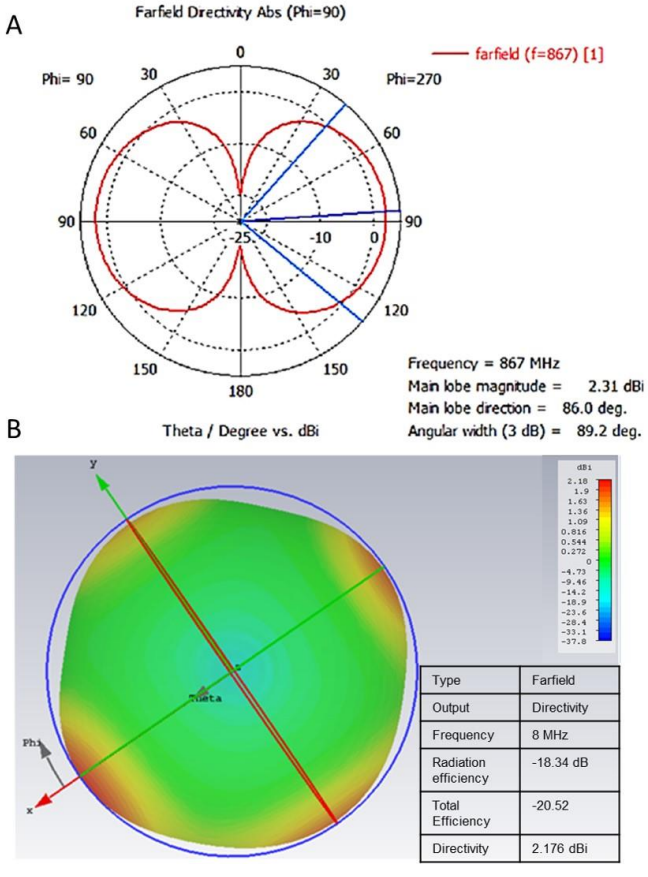

Figure 4 Antenna directivity of a voice prosthesis mounted UHF RFID convoluted antenna sensor within a gelatine phantom. A) The polar plot

This article has been accepted for publication in a future issue of this journal, but has not been fully edited. Content may change prior to final publication. Citation information: DOI 10.1109/JRFID.2020.3011900, IEEE Journal of Radio Frequency Identification

showed a 2.31 main lobe magnitude visualized with a phi 90° cut. B) The total efficiency and antenna directivity shown in a 3D model view.

An evident parallel exists with [18] when adjusting the body phantom for dielectric properties collected from other volunteer tissues (non-neck); done to determine if the sensor could be utilised within other body locations. A decrease in the dielectric properties from the pure muscle phantom (high dielectric) to volunteer tissue models (Table II) resulted in a downwards frequency shift (reduction in resonant frequency) (Fig. 5A). Similarly, as there was a reduction in conductivity (1 S/m in original gelatine phantom), the real part of impedance reduced leading to S11 matching near -10 dB (Fig. 5). As the S11 matching was better for the human tissue models at a lower permittivity, the UHF passive sensor should function with a higher efficiency for human tissue below pure muscle dielectric properties. Furthermore, only a capacitive adjustment of 2.6 pF would be required for volunteers one and two in order to shift the frequency resonance within the EU frequency band (Fig. 5). This could be easily done by the utilization of two device versions available based on the volunteer BMI and muscle to fat ratio appearance. Device implantation near tissues with pure muscle dielectric properties or a high body fluid contact location (blood vessels or with the bladder) could possibly just need the unaltered prototype as it functioned within the EU band without need for adjustment. Any other tissue implantation site would require the expressed capacitance increase of 2.6 pF.

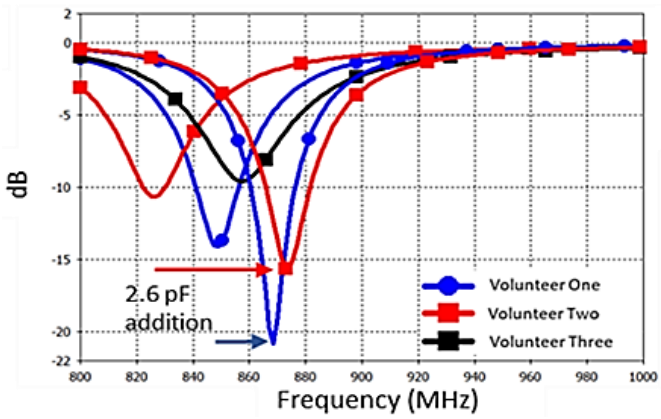

Figure 5 Wider dielectric range effect on presented design matching based on Table II volunteer data utilized within the simulated body phantom. With a decrease in the dielectric properties from the measured gelatine phantom, only volunteer three did not require a capacitive adjustment to remain within the EU frequency at resonance. For functioning with the UHF EU frequency band, volunteer one and two required a 2.6 pF shunt to adjust the resonant frequency (red and blue, respectively).

IV. CONCLUSION

The present UHF RFID sensor provided a read range near 65 cm with the EU frequency band and 80 cm within the US band and able to detect up to mature (30 µm) *C. albicans* biofilm thickness [3-6] upon a 10 µm polymer layer. With placement inserted within the neck, there is no necessary adjustments as neck dielectric data from volunteers (BMI range of 20.5 to 44.9) had negligible variability (Table I). Average neck permittivity only varied by ± 2.31 while conductivity varied by 0.64±0.058 suggesting only a single optimally tuned design could be possible for real life implementation within the neck for *C. albicans* biofilm growth detection upon a voice prosthesis. Within simulation this allowed for the use of a more accurate single human model for the effect of biofilm growth. For sensor implementation within other (non-neck) human tissues, the device would need an adjustment. With dielectric data collected from volunteer forearms (Table II; ranging permittivity from 22 to 42), the device should still be able to function within the EU UHF frequency band as needed. For optimal S11 matching, average to low muscle to fat ratio individuals would require a 2.6 pF additional shunt in the etched sensor as this device was originally intended for the (higher and less variable permittivity (Table I)) human neck. As the device was able to function when measured with a neck phantom suggest that with any necessary impedance matching adjustments, this device could detect microbial growth within other implantation sites. To make it less dependent on read-range, future adjustment would be necessary. Ultimately this presents a cost-effective approach to microbial detection upon an implantable device within a human host.

ACKNOWLEDGMENT

This work was funded by the UK Engineering and Physical Science Research Council (EPSRC). Conflict of interest: None declared.

REFERENCES

[1] Medical Implants Market - Forecasts from 2018 to 2023. Accessed: June 06, 2018. [Online]. Available at researchandmarkets.com/research .

[2] Global Next Generation Implants (NGI) Market –Analysis and Forecast (2017-2023) - Market Share Analysis and Competitive Insights. Accessed: June 06, 2018. [Online]. researchandmarkets.com/reports.

[3] Jakobsen, TH, Eickhardt, SR, Gheorghe, AG, Stenqvist, C, Sønderholm, M, Stavnsberg, C, Jensen, PØ, Odgaard, A, Whiteley, M, Moser, C, Hvolris, J, Hougen, HP, Bjarnsholt, T. Implants induce a new niche for microbiomes. APMIS 2018; 126: 685– 692.

[4] Fox EP, Nobile CJ. The role of *Candida albicans* biofilms in human disease. In: Dietrich LA, Friedmann TS, editors. Candida albicans symptoms, causes and treatment options. Nova Science Publishers; 2013. pp. 1–24.

[5] Gulati, Megha, and Clarissa J Nobile. "Candida albicans biofilms: development, regulation, and molecular mechanisms." Microbes and infection vol. 18,5 (2016): 310-21. doi:10.1016/j.micinf.2016.01.002

[6] Talpaert MJ, Balfour A, Stevens S, Baker M, Muhlschlegel FA, Gourlay CW (2015) Candida biofilm formation on voice prostheses. J Med Microbiol 64(Pt 3):199–208

[7] Potyrailo, R.A., et al., Battery-free radio frequency identification (RFID) sensors for food quality and safety. J Agric Food Chem, 2012. 60(35): p. 8535-43

[8] Yuan, M., E.C. Alocilja, and S. Chakrabartty, A Novel Biosensor Based on Silver-Enhanced SelfAssembled Radio-Frequency Antennas. IEEE Sensors Journal, 2014. 14(4): p. 941-942.

[9] Karuppuswami, S., et al., A Wireless RFID Compatible Sensor Tag Using Gold Nanoparticle Markers for Pathogen Detection in the Liquid Food Supply Chain. IEEE Sensors Letters, 2018. 2(2): p. 1-4.

[10] Mannoor, M.S., et al., Graphene-based wireless bacteria detection on tooth enamel. Nat Commun, 2012. 3: p. 763.

[11] Potyrailo, R.A., et al. Label-free biosensing using passive radio-frequency identification (RFID) sensors. in TRANSDUCERS 2009 - 2009 International Solid-State Sensors, Actuators and Microsystems Conference. 2009.

[12] B. D. Braaten and R. P. Scheeler, "Design of Passive UHF RFID Tag Antennas Using Metamaterial-Based Structures and Techniques," Radio Frequency Identification Fundamentals and Applications, Design Methods and Solutions, February, pp. 51–68, (2010).

[13] V. Makarovaite, A. J. R. Hillier, S. J. Holder, C. W. Gourlay and J. C. Batchelor, "Passive Wireless UHF RFID Antenna Label for Sensing Dielectric Properties of Aqueous and Organic Liquids," in IEEE Sensors Journal. [Online Early Access]

[14] V. Makarovaite, A. J. R. Hillier, S. J. Holder, C. Gourlay and J. C. Batchelor, "Voice Prosthesis Implantable UHF RFID Self-Sensing Tag for Microbial Growth Detection," 2019 IEEE International Conference on RFID Technology and Applications (RFID-TA), Pisa, Italy, 2019, pp. 314-317.

[15] Alien Technology, "Higgs-3 product overview". Available at http://www.alientechnology.com/products/ic/higgs-3, accessed 25 May 2017.

This article has been accepted for publication in a future issue of this journal, but has not been fully edited. Content may change prior to final publication. Citation information: DOI 10.1109/JRFID.2020.3011900, IEEE Journal of Radio Frequency Identification

[16] M.A. Ziai, J. C. Batchelor, "Temporary On-Skin Passive UHF RFID Transfer Tag", IEEE Transactions On Antennas And Propagation, Vol. 59, No. 10, October (2011).

[17] Junka AF, Janczura A, Smutnicka D, Mączyńska B, Anna S, Nowicka J, Bartoszewicz M, Gościniak G. Use of the Real Time xCelligence System for Purposes of Medical Microbiology. Pol J Microbiol. 2012 Sep 28;61(3):191197.

[18] SPEAG *Dak 3.5*. Accessed: June 06, 2019. [Online]. Available: https://www.speag.com/products/dak/dak-dielectric-probesystems/dak-3-5-200-mhz-20-ghz.

[19] Kamibayashi LK, Richmond FJ, "Morphometry of human neck muscles," in Spine (Phila Pa 1976). vol. 23, no. 12, pp. 1314-23 (1998).

[20] Q Duan, J H Duyn, N Gudino, J A de Zwart, P van Gelderen, "Characterization of a Dielectric Phantom for High-Field Magnetic Resonance Imaging Applications," Medical Physics, 41 (10), pp.102303-6, (2014).

[21] Voyantic Tagformance Pro. Accessed: June 06, 2018. [Online]. Available at https://voyantic.com/tagformance.

[22] G. A. Casula, "A Numerical Study on the Robustness of Ultrawide Band Wearable Antennas with respect to the Human Body Proximity," 2019 IEEE International Conference on RFID Technology and Applications (RFID-TA), Pisa, Italy, pp. 227-230 (2019).

[23] D. O. Oyeka, J. C. Batchelor and A. M. Ziai, "Effect of skin dielectric properties on the read range of epidermal ultra-high frequency radiofrequency identification tags," in Healthcare Technology Letters, vol. 4, no. 2, pp. 78-81, (2017).